JOURNAL OF MATERIALS SCIENCE 15 (1980) 2879–2883

The mechanics of crack initiation and propagation beneath a moving sharp indentor

J. C. CONWAY, Jr
Engineering Mechanics, The Pennsylvania State University, University Park, PA 16802, USA

H. P. KIRCHNER
Ceramic Finishing Company, State College, Pennsylvania, USA

The mechanics of crack initiation and propagation beneath a moving sharp indentor is investigated. Stresses generated beneath the indentor for selected horizontal-to-vertical load ratios are used in conjunction with an appropriate fracture mechanics solution to predict the propagation depth of penny cracks. Results predicted by the model are compared to those obtained in single point scratching and grinding experiments with soda lime glass.

1. Introduction

A need to optimize the processes associated with the shaping of brittle materials has generated a great deal of recent effort in the area of indentation fracture mechanics [1–5]. These investigations have focused on the fundamental phenomena associated with fracture initiation and propagation beneath both sharp and blunt indentors. They utilize a suitable elasticity solution for the stress field prior to initiation and a fracture mechanics solution to describe the propagation phase.

For the case of sharp indentors, the elastic stress field prior to fracture initiation has been described through classical elasticity solutions for point loading of a half-space such as the Boussinesq solution [6], the Mitchell solution [7] and the Mindlin solution [8]. For blunt indentors, the elastic stresses prior to fracture initiation are usually generated from the Hertz solution [9].

Initiation is assumed to take place at dominant flaws such as grain boundaries, inclusions or microcracks. Stable propagation following initiation can be treated in a more quantitative fashion by utilizing suitable fracture mechanics solutions to predict the extent of damage for a given flaw configuration, specimen geometry and loading condition [10, 11].

This paper treats the mechanics of crack initiation and propagation beneath a moving sharp indentor. The Mitchell solution [7] is used for the generation of the elastic stress field beneath the indentor for selected horizontal-to-vertical load ratios assuming a quasi-static loading condition. The stress field, for each load condition, is generated on planes parallel and perpendicular to the path of the moving indentor. Load ratios were selected to conform to the ranges encountered in single point scratching and grinding experiments previously conducted. Resultant stress fields beneath the indentor are examined to determine critical locations for fracture initiation under mode I and mixed-mode conditions. A stress intensity factor solution previously utilized by Lawn and Swain [3] is adopted to predict depth of damage for selected horizontal-to-vertical load ratios. Results predicted by the model are compared to those obtained in single point scratching and grinding experiments with soda lime glass.

2. Stress distributions

Referring to Fig. 1, the Mitchell solution was first utilized to generate the normal stresses σ_r, σ_θ, σ_ϕ and shear stress $\tau_{r\theta}$ in both the plane of motion of the indentor, $\phi = 0°$, and in the plane perpendicular to the plane of motion, $\phi = 90°$. The general form of the solution is given as

0022–2461/80/112879–05$02.50/0 © *1980 Chapman and Hall Ltd.*

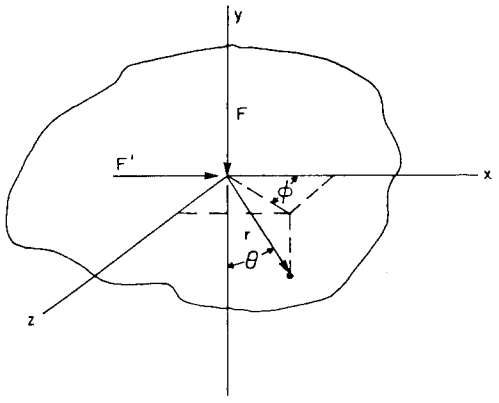

Figure 1 Coordinate system beneath moving indentor.

$$\sigma_{ij} = \left(\frac{F}{\pi r^2}\right)[f_{ij}(\theta, \phi)]_{\lambda,\mu} + \left(\frac{F'}{\pi r^2}\right)[g_{ij}(\theta, \phi)]_{\lambda,\mu} \quad (1)$$

where F is the vertical load, F' is the horizontal load, λ and μ are Lame's constants, and r, θ and ϕ represent the polar coordinates.

Resultant non-dimensionalized stresses in the plane of motion of the indentor are shown in Fig. 2 for selected horizontal-to-vertical load ratios. These results should be interpreted with special attention being given to regions of relatively high tensile stresses, as these stresses are likely to lead to crack initiation and propagation. Thus, the radial stresses σ_r in the region behind the contact point increase positively with increasing horizontal-to-vertical load ratio leading one to expect crack initiation and propagation perpendicular to the track. Lawn and Wilshaw [12] illustrated cracks of this type. Similarly, the in-plane hoop stresses σ_θ show increasing tensile values ahead of the contact point with a corresponding increase in in-plane shearing stresses for increasing horizontal-to-vertical load ratios. This stress state could lead to mixed-mode fracture resulting in chip removal and can be investigated with appropriate fracture mechanics solutions [13–15]. Finally, the out-of-plane hoop stresses σ_ϕ show a tensile stress increase ahead of the contact point for increasing horizontal-to-vertical load ratio. This stress is expected to cause initiation and propagation of median cracks beneath the tool. These cracks are principally responsible for strength degradation and were selected as the major topic of this investigation. Stress distributions in the plane perpendicular to the plane of motion of the indentor were found to be independent of the horizontal force and are given by the curves labelled $F' = 0$ in Fig. 2.

3. Failure model

The failure model assumes that median vent cracks are adequately modelled as embedded penny cracks. The penny cracks are assumed to initiate on the boundary of a disturbed (plastically deformed and locally shear cracked) zone extending a distance Z_o beneath the surface and propagate to a final distance c as shown in Fig. 3 for $\phi = 0°$. Utilizing an approach similar to Lawn and Swain [3], the stress intensity factor for this case is given as

$$K_I = \frac{2^{1/2}}{\pi}\left[2\left(\frac{c}{\pi}\right)^{1/2}\int_{Z_o}^{c}\frac{\sigma_\phi(r)\mathrm{d}r}{(c^2 - r^2)^{1/2}}\right]. \quad (2)$$

Examination of this expression indicates that the stress intensity factor is dependent on the depth of the disturbed zone, Z_o, and the out-of-plane hoop stress distribution, $\sigma_\phi(r)$, beneath the tool.

The parameter Z_o, representing the lower limit of the integral in Equation 2, is assumed to be primarily dependent on shear flow and cracking along the maximum shear stress trajectories beneath the tool. Physical evidence of such flow and precracking prior to initiation and subsequent propagation of penny cracks for sharp indentors has been shown by Swain [16]. Assuming that the extent of disturbed zone is controlled by the magnitude of the maximum shear stress beneath the tool and the critical mode II stress intensity factor, K_{IIc} one can define a parametric relationship for the extent of shear flow and cracking by utilizing Equation 1 and the expression for the maximum shear stress as

$$\tau_{max} = \pm\left[\left(\frac{\sigma_r - \sigma_\theta}{2}\right)^2 + \tau_{r\theta}{}^2\right]^{1/2}. \quad (3)$$

Such a computation directly beneath the indentor ($\theta = 0°$) for either the plane of motion ($\phi = 0°$) or the plane perpendicular to the plane of motion ($\phi = 90°$) indicates that

$$Z_o \propto F^{1/2}. \quad (4)$$

The extent of shear flow and cracking prior to initiation of the penny crack is thus controlled by the square root of the vertical load. Computations also indicate that the horizontal load component has

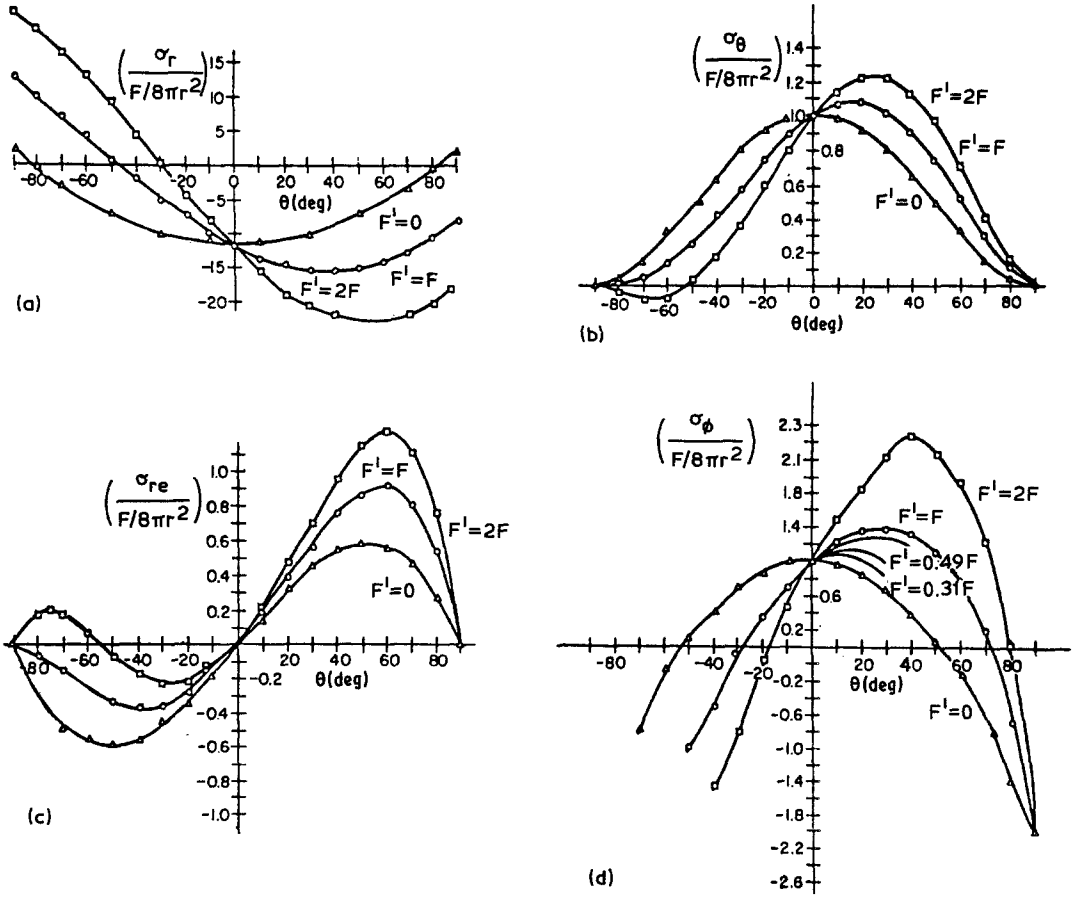

Figure 2 Non-dimensionalized stresses in plane of motion of indentor for selected load ratios.

very little influence on the extent of the disturbed zone directly beneath the indentor.

The out-of-plane hoop stress for the plane $\phi = 0°$ directly beneath the indentor ($\theta = 0°$) is given as

$$\sigma_\phi(r) = \frac{FQ}{8\pi r^2} \tag{5}$$

where F is the vertical load, r the distance beneath the indentor, and Q a factor which represents the increase in out-of-plane hoop stress for a corresponding increase in horizontal-to-vertical load ratio. This increase, indicated in Fig. 2d for horizontal-to-vertical load ratios considered in this investigation, is shown in Table I.

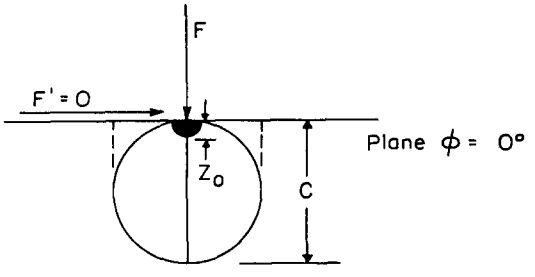

Figure 3 Assumed relationship of disturbed zone and penny crack beneath tool.

Substitution of Equation 5 into Equation 2 and integrating gives

$$K_I = \frac{0.02\,FQ}{(c^{1/2}Z_o)} \tag{6}$$

Introducing the mode I critical stress intensity factor K_{IC}, an expression for the maximum propagation depth of the penny crack is obtained as

$$c = \frac{0.02\,FQ^2}{K_{IC}Z_o}. \tag{7}$$

TABLE I Effect of load ratio on out-of-plane hoop stress

Load Ratio (F'/F)	Location of Maximum (σ_ϕ)	Q
0	0°	1.00
1	30°	1.40
2	40°	2.25

The depth of damage is thus seen to increase with a corresponding increase in horizontal load (increased Q) and the penny cracks are shown to be shifted forward ahead of the tool. For materials with extensive shear flow and cracking (large Z_o), the depth of damage and resultant strength degradation will be reduced.

For the plane perpendicular to the plane of motion of the tool, the horizontal load does not affect the out-of-plane hoop stress ($Q = 1$) indicating that the penny cracks will propagate to greater lengths in the plane of motion of the tool. Mecholsky, Freiman, and Rice [17] have shown that glass specimens fractured by stresses applied perpendicular to the (multipoint) grinding direction fail at lower stresses than those in which the applied stresses are parallel to the grinding direction. This result indicates that cracks in the plane of motion of the tool are deeper than those perpendicular to this plane.

4. Experimental evaluation

The failure model was evaluated using data from scratching and single point grinding experiments on soda lime glass [18]. Glass plates (10.5 cm × 4.5 cm × 0.6 cm) were scratched by 75° cone wheel dressers using four ratios of horizontal-to-vertical load and the depth of damage was measured. In the case of the grinding experiments, soda lime glass plates (13.0 cm × 5.2 cm × 6.4 cm) were machined by single point grinding. Horizontal-to-vertical load ratios achieved during grinding were recorded and the depth of damage was again measured.

Comparison of predicted and measured results was made by rewriting Equation 7 as

$$\frac{FQ}{Z_o} = \frac{K_{IC}}{0.02} c^{1/2} \tag{8}$$

where $K_{IC}/0.02 = 3.5 \times 10^7 \mathrm{PaM}^{1/2}$ for soda lime glass. Experimental data is compared to Equation 8 in Fig. 4 for both the scratching and single point grinding tests. Experimental and predicted results show reasonable agreement.

5. Discussion and conclusions

The mechanics of fracture initiation and propagation beneath moving diamond tools can be adequately described by fracture mechanics analysis. The analysis involves the use of the Mitchell Solution for the determination of stress distributions beneath the indentor for selected horizontal-to-vertical load ratios and a fracture mechanics solution for embedded penny cracks. Shear flow and cracking prior to initiation is considered as is the effect of the horizontal-to-vertical load ratio.

The analysis also shows that the horizontal load imparted to the specimen does not influence stresses perpendicular to the plane of motion of the tool. Therefore, horizontal loads are not expected to influence crack initiation and propagation in the plane perpendicular to the plane of motion.

The investigation also defines two other failure modes. The first, associated with the radial stress distribution behind the tool, is expected to result in U-shaped cracks in the track. The second, associated with the in-plane hoop and shear stresses ahead of the tool, should result in mixed mode failure and chipping to the surface. Both of these topics will be the subject of future investigations.

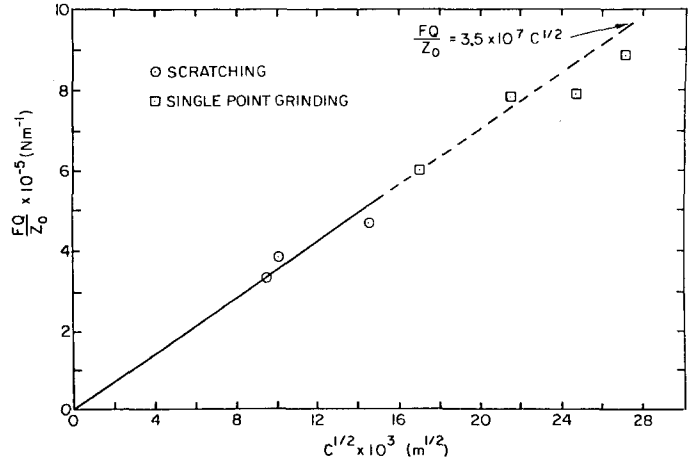

Figure 4 FQ/Z_o versus $c^{1/2}$ for scratching and single point grinding of glass plates.

In addition, future investigations will be directed toward an improved understanding of shear flow and cracking in the disturbed zone as it is felt that crack initiation sites for many significant failure modes are located in this region.

Acknowledgements

The authors are pleased to acknowledge the contributions of their associates at Ceramic Finishing Company, especially D. M. Richard and E. A. Isaacson and the sponsorship of the National Science Foundation under contract DAR 78-18091.

References

1. B. R. LAWN and E. R. FULLER, *J. Mater. Sci.* **10** (1975) 2016.
2. B. R. LAWN and T. R. WILSHAW, *ibid.* **10** (1975) 1049.
3. B. R. LAWN and M. V. SWAIN, *ibid.* **10** (1975) 113.
4. B. R. LAWN, S. M. WIEDERHORN and H. H. JOHNSON, *J. Amer. Ceram. Soc.* **58** (1975) 428.
5. B. R. LAWN, E. R. FULLER and S. M. WIEDERHORN, *ibid.* **59** (1976) 193.
6. S. TIMOSHENKO and J. N. GOODIER, "Theory of Elasticity" (McGraw-Hill, New York, 1951) p. 362.
7. J. H. MITCHELL, Proceedings of the London Mathematical Society, **52** (1900) 35.
8. R. D. MINDLIN, *Physics* 7 (1936) 195.
9. H. HERTZ, *J. Math. (Crelle's J.)* **92** (1881).
10. P. C. PARIS and G. C. SIH, *ASTM STP* **361** (1968) 30.
11. H. TADA, P. C. PARIS and G. R. IRWIN, "The Stress Analysis of Cracks Handbook" (Del Research Corporation, Hellertown, PA, 1973) pp. 2–24.
12. B. R. LAWN and T. R. WILSHAW, "Fracture of Brittle Solids" (Cambridge University Press, Cambridge, 1975) p. 65.
13. P. C. PARIS and G. C. SIH, *ASTM STP* **381** (1965) 40.
14. D. HOYNIAK and J. C. CONWAY, *Eng. Fract. Mec.* **12** (1979) 301.
15. G. C. SIH, *Int. J. Fract.* **10** (1974) 305.
16. M. V. SWAIN, *J. Amer. Ceram. Soc.* **62** (1979) 318.
17. J. J. MECHOLSKY, S. W. FREIMAN and R. W. RICE, Eleventh International Congress on Glass (Prague, Czechoslovakia, 1977).
18. H. P. KIRCHNER, R. M. GRUVER and D. M. RICHARD, *NBS Special Publication* **526** (1979) 23-42.

Received 27 March and accepted 1 May 1980.